EPR Studies of Amine Radical Cations. Part 2. Thermal and Photo-Induced Rearrangements of Propargylamine and Allylamine Radical Cations in Low-Temperature Freon Matrices

Wolfgang Knolle,* Igor Janovský, and Sergej Naumov

Leibniz-Institut für Oberflächenmodifizierung (IOM), Permoserstr.15, D-04303 Leipzig, Germany

Ffrancon Williams

Department of Chemistry, University of Tennessee, 1420 Circle Drive, Knoxville, Tennessee 37996-1600

Received: July 28, 2006; In Final Form: October 12, 2006

Matrix EPR studies and quantum chemical calculations have been used to characterize the consecutive H-atom shifts undergone by the nitrogen-centered parent radical cations of propargylamine (**1b**$^{\bullet+}$) and allylamine (**5**$^{\bullet+}$) on thermal or photoinduced activation. The radical cation rearrangements of these unsaturated parent amines occur initially by a 1,2 H-atom shift from C1 to C2 with π-bond formation at the positively charged nitrogen; this is followed by a consecutive reaction involving a second H-atom shift from C2 to C3. Thus, exposure to red light ($\lambda > 650$ nm) converts **1b**$^{\bullet+}$ to the vinyl-type distonic radical cation **2**$^{\bullet+}$ which in turn is transformed on further photolysis with blue-green light ($\lambda \approx 400-600$ nm) to the allene-type heteroallylic radical cation **3**$^{\bullet+}$. Calculations show that the energy ordering is **1b**$^{\bullet+}$ > **2**$^{\bullet+}$ > **3**$^{\bullet+}$, so that the consecutive H-atom shifts are driven by the formation of more stable isomers. Similarly, the parent radical cation of allylamine **5**$^{\bullet+}$ undergoes a spontaneous 1,2-hydrogen atom shift from C1 to C2 at 77 K with a $t_{1/2}$ of ∼1 h to yield the distonic alkyl-type iminopropyl radical cation **6**$^{\bullet+}$; this thermal reaction is attributed largely to quantum tunneling, and the rate is enhanced on concomitant photobleaching with visible light. Subsequent exposure to UV light ($\lambda \approx 350-400$ nm) converts **6**$^{\bullet+}$ by a 2,3 H-shift to the 1-aminopropene radical cation **7**$^{\bullet+}$, which is confirmed to be the lowest-energy isomer derived from the ionization of either allylamine or cyclopropylamine. Although the parent radical cations of *N*, *N*-dimethylallylamine (**9**$^{\bullet+}$) and *N*-methylallylamine (**11**$^{\bullet+}$) are both stabilized by the electron-donating character of the methyl group(s), the photobleaching of **9**$^{\bullet+}$ leads to the remarkable formation of the cyclic 1-methylpyrrolidine radical cation **10**$^{\bullet+}$. The first step of this transformation now involves the migration of a hydrogen atom to C2 of the allyl group from one of the methyl groups (rather than from C1); the reaction is then completed by the cyclization of the generated $MeN^{+}(=CH_2)$ $CH_2CH_2CH_2^{\bullet}$ distonic radical cation, possibly in a concerted overall process. In contrast to the ubiquitous H-atom transfer from carbon to nitrogen that occurs in the parent radical cations of saturated amines, the alternate rearrangements of either **1b**$^{\bullet+}$ or **5**$^{\bullet+}$ to an ammonium-type radical cation by a hypothetical H-atom shift from C1 to the ionized NH_2 group are not observed. This is in line with calculations showing that the thermal barrier for this transformation is much higher (∼120 kJ mol^{-1}) than those for the conversion of **1b**$^{\bullet+}$ → **2**$^{\bullet+}$ and **5**$^{\bullet+}$→ **6**$^{\bullet+}$ (∼40−60 kJ mol^{-1}).

Introduction

The important role played by the electron-transfer reactions of amines in a wide variety of synthetic, biological, and technological applications has been documented in several recent reviews.[1−4] In this contribution, we extend our EPR studies of primary alkylamine radical cations described in the previous paper[5] to examine the radiolytic oxidation of propargylamine, allylamine, and closely related compounds. These amines possess highly reactive functional groups, and together with cyclopropylamine, they and their derivatives feature prominently as efficient inactivators of enzymes such as monoamine oxidase and cytochrome P-450.[3b−d] Consistent with an enzymatic one-electron oxidation process, the aminium radical cations that are formed in this case are considered to undergo a "mechanism-based rearrangement" to form highly reactive xenobiotic species.[3c] For example, enzyme inactivation by cyclopropylamines is generally considered to result from the ring opening of the primary nitrogen-centered radical cation to an alkyl-type radical that can attack the active site of the enzyme.[3b−d] *N*,*N*-Dimethylpropargylamine has also been shown to function as an efficient enzyme inactivator;[3e,f] however, at least three possible mechanisms of inactivation could account for the structure of the covalent flavin-inhibitor adduct formed in this case, and it was not possible to distinguish between them on the basis of the biochemical studies.[3f] Therefore, additional basic information on the oxidation chemistry of these amines is desirable. These particular amines have also found application in plasma polymerization designed to bring about the amino-functionalization of polymer surfaces. This technique is of interest in applications to promote adhesion and for improving the biocompatibility of artificial biomaterials. Radical cations are again key intermediates, and their stability and possible rearrangement reactions may determine the kind of functional groups present on the surface of the polymer deposited by the

* To whom correspondence should be addressed. Fax: (+49) 341 2352584. E-mail: wolfgang.knolle@iom-leipzig.de.

10.1021/jp064825s CCC: $33.50
Published on Web 12/07/2006

plasma. A study of the plasma-deposited films derived from the polymerization of propyl, allyl, and propargyl amines was presented by Fally,[6] but no effort was made to link the observed differences to the possible reaction steps following primary ionization.

Matrix EPR,[7a,8] mass-spectrometric,[7b,c] as well as detailed computational studies[7d] have previously been reported on the rearrangement of the parent cyclopropylamine and allylamine radical cations to give the same distonic $^{\bullet}CH_2CH_2CH{=}NH_2^+$ species. For cyclopropylamine, the rearrangement occurs by ring opening at the amine-substituted carbon,[7] whereas for allylamine, the reaction takes place by a 1,2 hydrogen-atom shift.[8] Under mass-spectrometric conditions, however, the distonic species was found to further rearrange by a 1,2-hydrogen shift to the more stable 1-aminopropene radical cation.[7b,d]

In the previous matrix EPR work on cyclopropylamine and allylamine,[7a,8] the primary nitrogen-centered radical cations were not observed, and only the secondary distonic radical cation was identified in each case. Clearly, if the rearrangements occur rapidly at 77 K, the use of lengthy gamma-irradiation exposures at low dose rates prior to EPR observation precludes the detection of the primary species. On the other hand, since electron-beam irradiation can deliver high doses in short times (ca. 1 min), direct EPR observations can be made in favorable cases on the kinetics of thermal transformations involving the primary radical cation.[9] For example, in a recent study on the radiolytic oxidation of 2,5-dihydrofuran,[9a] this technique allowed the decay ($t_{1/2}$ of 3−4 min at 77 K, depending on the Freon matrix) of the oxygen-centered primary radical cation to the distonic 2,4-dihydrofuran species to be followed by kinetic EPR spectroscopy. Using this methodology, we have investigated the radiolytic oxidation of propargylamine, allylamine, and its methyl and dimethyl derivatives and now report in detail on the thermal and photoinduced transformations of their radical cations.

Experimental Section

Materials. Allylamine (98% +, Lancaster), *N*-methylallylamine (96%, Aldrich), *N*,*N*-dimethylallylamine (98% +, Merck), *N*-methylpyrrolidine (97%, Aldrich), and propargylamine (99.1% according to GC analysis, Sigma) were used as received. *N*,*N*-Dideuterioallylamine was prepared from the corresponding protiated compound by hydrogen exchange with heavy water (99.5% according to NMR); the mixture of amine with excess of D_2O (tenfold in mol) was stirred for about 20 h at room temperature; amine was then separated by distillation, and the procedure was repeated once more. The content of the deuterated compound in the final reaction product of ≥98% was estimated by NMR. 1,1,1-Trifluorotrichloroethane (99%, Aldrich or Acros) was purified by passing it through a column filled with neutral Al_2O_3. 1,1,2-Trifluorotrichloroethane (Uvasol 99,9%, Merck) was used as supplied.

Sample Preparation and Irradiation. Amines were dissolved in freons at solute to solvent concentrations typically between about 1:500 and 1:1000 and carefully degassed by the freeze−thaw technique. The solutions were irradiated in the dark at 77 K in liquid nitrogen with the electron beam of a Linac (Elektronika U-003, Thorium, Moscow). A dose of ≈10−15 kGy (irradiation time approximately 1 min) was sufficient to generate a well observable concentration of paramagnetic species. Irradiated samples were protected from light and the first spectrum was taken as soon as possible (within about 2.5 min) after irradiation.

EPR Spectroscopy. The measurements were performed using a Bruker ESP 300e spectrometer (9.5 GHz, 100 kHz modulation) equipped with either a finger Dewar (77 K) or a variable temperature control unit (ER 4121 VT, at ≥95 K). Spectra were recorded at a microwave power of 0.1 mW and a modulation amplitude of 0.05 or 0.1 mT.

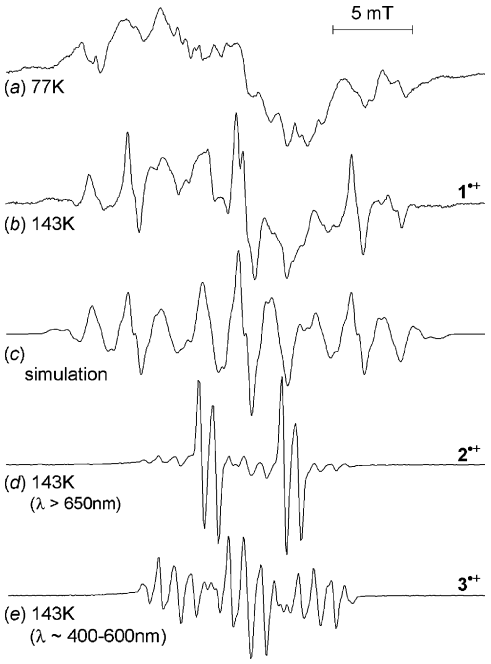

Figure 1. EPR spectra of a frozen solution (1:500) of propargylamine in CF_3CCl_3 irradiated at 77 K and measured at the temperatures indicated. Spectra d and e are obtained after photobleaching at 77 K with red and subsequently blue-green light, respectively. For parameters for simulation c, see text.

Sample Photobleaching. A tungsten lamp (250 W) and a Xenon lamp (XBO 1000 W, Osram) equipped with a water heat-filter and colored glass filters were used for sample illumination at 77 K (outside the EPR cavity).

Spectra Simulations. Isotropic and anisotropic spectra simulations were performed using the *WinSim*[10] and *SimFonia* (BRUKER) software, respectively.

Theoretical Calculations. Quantum chemical calculations were performed using density functional theory (DFT) hybrid B3LYP[11a,b] methods with the standard 6-31G(d) basis set as implemented in the Gaussian 03 program.[12] It was shown[13] that B3LYP and several other DFT functionals (which set the HF exchange equal to 20%) tend to delocalise spin for radical cation structures where localization of the unpaired electron is expected. Therefore, calculations with the BH&HLYP method,[11c] which utilizes a larger fraction of the HF exchange (50%), were made for comparison. Both B3LYP and BH&HLYP methods produce qualitatively similar geometrical and electronical molecular parameters. However, the hfs constants calculated with B3LYP are in slightly better agreement with the experiment.

Results and EPR Spectral Assignments

Propargylamine (PAA). The spectrum observed after irradiation of a PAA solution in CF_3CCl_3 at 77 K in the dark (Figure 1a) is a broad multiplet with an overall width of 27 mT. Increasing the temperature to 143 K results in improved resolution and a slight reduction in spectral width (25 mT), but even at this temperature, the anisotropic contributions are not fully averaged (Figure 1b). The change is completely reversible since the original spectrum is regenerated on recooling the sample to 77 K. It is also noteworthy that the steel-blue color of the sample persists over this temperature range and disappears

TABLE 1: Spin Density (ρ), Mulliken Charge Distribution (q), and Coupling Constants a/mT for the Propargylamine Radical Cation $\mathbf{1}^{\bullet+}$ and Its Isomers, Calculated with B3LYP/6-31G(d,p)[a]

	$\mathbf{1a}^{\bullet+}$	$\mathbf{1b}^{\bullet+}$		$\mathbf{2}^{\bullet+}$		$\mathbf{3}^{\bullet+}$		$\mathbf{4}^{\bullet+}$
	calc	calc	exp	calc	exp	calc	exp	calc
$\Delta E(E_0+ZP)$	+3.99			-105.2		-151.2		-60.7
ρ(N)	**0.690**	**0.686**		-0.035		**0.398**		-0.035
ρ(C1)	-0.015	-0.017		0.025		0.064		**0.723**
ρ(C2)	0.049	0.020		-0.136		**0.568**		-0.285
ρ(C3)	0.329	0.162		**1.078**		-0.093		**0.624**
q(N)	0.359	0.363		0.232		0.279		0.597
q(C1)	0.300	0.333		0.463		0.300		0.063
q(C2)	0.221	0.279		0.079		0.297		0.325
q(C3)	0.120	0.024		0.226		0.123		0.014
a(N)[b]	3.32/0.03 (1.13)	3.31/0.22 (1.25)	2.5/1.5	-0.18/0.02 (-0.07)		1.98/0.21 (0.80)	1.28/0.75	-0.39/-0.21 (-0.27)
a(H,N)	-1.74 (2H)	-1.77 (2H)	2.45 (2H)	0.11/0.09		-1.12 (2H)	1.02 (2H)	1.16 (3H)
a(H,C1)	0.11/0.12	9.10/9.16	7.10 (2H)	-0.06		-0.17	-	-2.01
a(H,C2)	-	-	-	5.02	5.17	-	-	-
a(H,C3)	-0.96	-0.46	0.40	0.84	0.89	4.10 (2H)	4.38 (2H)	-0.17
λ/nm	525 (0.093) 236 (0.003)	839 (0.053) 223 (0.003)		327 (0.002) 218 (0.381)		277 (0.003) 269 (0.019)		301 (0.037) 254 (0.002)

[a] Data are given for the most stable conformer. Relative stability ΔE/kJ mol^{-1} (including zero point vibrational energy) is calculated with respect to isomer $\mathbf{1b}^{\bullet+}$. Wavelengths λ/nm (calculated with B3LYP/6-311+G(d,p)) correspond to the transitions with lowest energy showing significant intensity (oscillator strength given in brackets). [b] Anisotropy for nitrogen coupling is given as $a_{||}/a_{\perp}$; a_{iso} (given in brackets) = 1/3 ($a_{||} + 2a_{\perp}$).

TABLE 2: Calculations Performed with BH&HLYP/6-31G(d,p)[a]

	$\mathbf{1a}^{\bullet+}$	$\mathbf{1b}^{\bullet+}$		$\mathbf{2}^{\bullet+}$		$\mathbf{3}^{\bullet+}$		$\mathbf{4}^{\bullet+}$
	calc	calc	exp	calc	exp	calc	exp	calc
ΔE (E_0+ZP)	+ 1.88			−123.0		−157.0		−77.1
ρ(N)	**0.804**	**0.934**		−0.047		**0.421**		−0.048
ρ(C1)	−0.020	−0.053		0.031		0.005		**0.815**
ρ(C2)	−0.039	−0.003		−0.191		**0.656**		−0.432
ρ(C3)	0.322	0.030		**1.144**		−0.142		**0.702**
q(N)	0.404	0.484		0.208		0.267		0.595
q(C1)	0.338	0.349		0.507		0.351		0.122
q(C2)	0.137	0.165		0.045		0.232		0.230
q(C3)	0.119	0.01		0.239		0.150		0.701
a(N)[b]	4.16/0.38 (1.64)	4.71/0.85 (2.14)	2.5/1.5	−0.27/−0.04 (−0.16)		2.47/0.45 (1.12)	1.28/0.75	−0.38/−0.34 (−0.35)
a(H,N)	−2.37 (2H)	−2.80/−2.72	2.45 (2H)	0.15/0.14		−1.41 (2H)	1.02 (2H)	1.19 (3H)
a(H,C1)	0.16 (2H)	7.48 (2H)	7.10 (2H)	−0.08		0.03		−2.43
a(H,C2)				4.99	5.17			
a(H,C3)	−1.03	−0.09	0.40	0.54	0.89	4.12 (2H)	4.38 (2H)	−2.03

[a] For details, see Table 1. [b] Anisotropy for nitrogen coupling is given as $a_{||}/a_{\perp}$; a_{iso} (given in brackets) = 1/3 ($a_{||} + 2a_{\perp}$).

only on photobleaching. A similar EPR spectrum is observed in $CFCl_2CF_2Cl$ at 77 K but with much poorer resolution; the spectrum persists at 77 K but disappears quickly on raising the temperature above the matrix softening point (~105 K). This decay can be attributed to bimolecular ion−molecule reactions which can occur in $CFCl_2CF_2Cl$ between 80 and 130 K, depending on the solute.[14]

The spectra shown in Figure 1a,b can be readily assigned to the primary radical cation of propargylamine $\mathbf{1}^{\bullet+}$. Quantum chemical calculations (Tables 1 and 2) show that most of the spin density for this radical cation is localized at nitrogen, and as in the case of *n*-propylamine,[5] two stable conformers ($\mathbf{1a}^{\bullet+}$ and $\mathbf{1b}^{\bullet+}$) are predicted, which differ mainly by the orientation of the π-radical at the (nearly planar) NH_2 group to the neighboring methylene group (Scheme 1).

The eclipsed conformer $\mathbf{1b}^{\bullet+}$ with the larger β-proton couplings ($2H_\beta$, B3LYP: 9.13 mT or BH&HLYP: 7.48 mT)

SCHEME 1

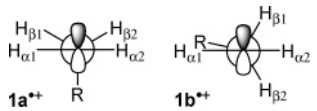

is found to be more stable than conformer $\mathbf{1a}^{\bullet+}$ by −4 (B3LYP) or −1.9 kJ mol^{-1} (BH&HLYP, see Tables 1 and 2), respectively, and can account for the observed large spectral width. Indeed, a satisfactory best-fit powder simulation (Figure 1c) is obtained by combining the isotropic coupling constants of 7.1 mT ($2H_\beta$) and 0.4 mT ($1H_\delta$) for the more remote β and δ hydrogens with the anisotropic couplings of 2.6, 2.2, and 2.2 mT ($2H_\alpha$) and 2.5, 1.5, and 1.5 mT (1N) for the α-protons and nitrogen, respectively. Moreover, since calculations of allowed optical transitions predict that the primary radical cation $\mathbf{1}^{\bullet+}$ is the only $C_3H_5N^{\bullet+}$ isomer with a significant absorption band in the red

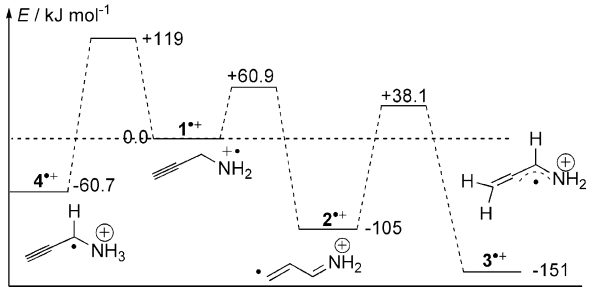

Figure 2. Energy diagram $\Delta(E_0 + \mathrm{ZPE})$ of transformations of the propargylamine radical cation, calculated with B3LYP/6-31G(d,p).

spectral range (500−800 nm), the assignment is also supported by the observed (complementary) blue color and the photosensitivity of $\mathbf{1}^{\bullet+}$ to visible light, as described below.

Exposure of the PAA sample of $\mathbf{1}^{\bullet+}$ at 77 K in CF_3CCl_3 to red light ($\lambda > 650$ nm) leads to a completely different spectrum dominated by the sharp lines from a doublet of doublets (Figure 1d). This spectrum is stable up to 143 K, except for a reversible slight reduction in the line width. On further illumination (at 77 K) with blue-green light ($\lambda \approx 400-600$ nm), a third spectrum (Figure 1e) grows in, these consecutive phototransformations proceeding from $\mathbf{1}^{\bullet+}$ without significant loss of spin concentration (<10%). Comparison at 143 K of the well-resolved spectrum taken after exposure to red light with the one obtained by subsequent blue-green light illumination shows that the latter spectrum (Figure 1e) is already present to a certain extent (<40%) in the spectrum of Figure 1d, as expected for consecutive reactions. To assist in the assignment of these two new spectra, we turn to examine the ground state energies (Figure 2) and coupling constants (cf. Tables 1 and 2) predicted by quantum chemical calculations for the possible stable isomers of the primary radical cation $\mathbf{1}^{\bullet+}$.

Considering first the possibility of a H-shift from C1 to the adjacent NH_2 group, the enthalpy change (−60.7 kJ mol^{-1}) is favorable but this rearrangement leading to radical cation $\mathbf{4}^{\bullet+}$ would have to overcome an exceedingly high barrier (+119 kJ mol^{-1}) in a ground-state reaction. This does not, of course, preclude its formation via 650 nm photoexcitation (184 kJ mol^{-1}), but as the expected splitting pattern (Tables 1 and 2) for $\mathbf{4}^{\bullet+}$ does not fit either of the observed spectra (Figure 1d,e), its formation can almost certainly be ruled out in the present work.

On the other hand, a 1,2-H shift from C1 to C2 at the unsaturated (triple) bond (Scheme 2) analogous to that observed thermally for the allylamine[8] radical cation (vide infra) leads to the vinyl-type radical cation $\mathbf{2}^{\bullet+}$, for which the measured doublet splitting constants of 5.17 and 0.89 mT (Figure 1d) agree very well with the calculated values (B3LYP: 5.02 and 0.84 mT for the β and α protons, respectively). Since other vinyl radicals with the spin localized in a σ orbital on the terminal carbon invariably show β-proton couplings in the range of 4−6 mT (with $a(\beta\text{-H}_{anti}) > a(\beta\text{-H}_{syn})$) due to strong hyperconjugation,[15] the assignment to $\mathbf{2}^{\bullet+}$ is definitive. Therefore, the first photorearrangement process induced efficiently by low-energy (184 kJ mol^{-1}) photons can be confidently attributed to the $\mathbf{1}^{\bullet+} \rightarrow \mathbf{2}^{\bullet+}$ transformation.

Interestingly, this rearrangement is calculated (Figure 2) to have a much lower adiabatic barrier (+60.9 kJ mol^{-1}) than that (+119 kJ mol^{-1}) for $\mathbf{1}^{\bullet+} \rightarrow \mathbf{4}^{\bullet+}$, although it is debatable whether this consideration plays a key role in determining the overall photochemistry.

Turning now to the second photorearrangement produced by exposure of the radical cation $\mathbf{2}^{\bullet+}$ to light of shorter-wavelengths (200−300 kJ mol^{-1}), there is good agreement between the coupling constants derived from the experimental spectrum in Figure 1e (a/mT: 4.38 (2H), 1.02 ($2H_N$), and 0.93 (N_{iso})) and the B3LYP calculated (a/mT: 4.10 (2H), 1.12 ($2H_N$), and 0.8 (N_{iso})) coupling constants (Table 1) for the allene-type isomer $\mathbf{3}^{\bullet+}$. The spin in $\mathbf{3}^{\bullet+}$ is distributed over a delocalized heteroallylic structure involving the amine terminus of this allene-type radical cation (see Table 1 and 2), and this structure nicely accounts for the large coupling to the two β-hydrogens on C3 through efficient hyperconjugation from spin density on C2. Also, the nodal character of this allylic-type orbital is consistent with both the lack of significant coupling to the hydrogen on C1 and the presence of significant spin density on nitrogen. The latter is revealed by the partial anisotropy at nitrogen (Figure 1e) that remains even at 143 K, where the finer details of the spectrum can only be perfectly reproduced by using the axial hyperfine components $a_{||} = 1.28$ mT and $a_{\perp} = 0.75$ mT instead of the isotropic $a(N_{iso})$ value of 0.93 mT. Accordingly, we confidently assign $\mathbf{3}^{\bullet+}$ as the product of photoisomerization of $\mathbf{2}^{\bullet+}$, a process that can occur by a simple 2,3-H shift (Scheme 3).

Allylamine−Kinetics of the Spontaneous Intramolecular H-Shift. Previous studies have investigated the EPR spectra obtained after γ-irradiation of allylamine/freon solutions at 77 K in some detail.[8] Although the primary radical cation $\mathbf{5}^{\bullet+}$ could not be detected, the observed spectrum was unambiguously assigned to the distonic iminopropyl radical cation $\mathbf{6}^{\bullet+}$, its formation being attributed to the rearrangement of $\mathbf{5}^{\bullet+}$ resulting from a 1,2 H-shift to the vinyl group (Scheme 4).

Since irradiation periods on the order of at least 1 h are generally required with most γ sources to obtain a sufficient dose (2−5 kGy or 0.2−0.5 Mrad) for EPR signal detection, any rearrangement of the primary species that takes place on a shorter time scale cannot be followed kinetically. Thus, in the previous work,[8] the observation of an unchanging strong signal from $\mathbf{6}^{\bullet+}$ implies that the complete conversion of $\mathbf{5}^{\bullet+}$ to $\mathbf{6}^{\bullet+}$ had essentially occurred during the time (ca. 6 h) of γ irradiation. Recent work[9] has shown, however, that this experimental limitation of γ irradiation can be overcome by the use of high-energy electron irradiation which can deliver a similar dose within about a minute, thus greatly extending the experimental time window for monitoring the kinetics of a fast rearrangement process. It was therefore of interest to determine whether the primary radical cation of allylamine $\mathbf{5}^{\bullet+}$ can be observed by means of this e-beam technique and, if so, to determine the kinetics of its transformation to $\mathbf{6}^{\bullet+}$.

The EPR spectrum observed 1.5 min after electron-beam irradiation of frozen allylamine/CF_3CCl_3 solution at 77 K is shown by the dotted line in Figure 3a. Signals from the secondary distonic species $\mathbf{6}^{\bullet+}$ are present as before,[8] but in this case, their intensity grows with time (by a factor of ∼5) to reach a limiting value after 3 h (cf. Figure 4). This final spectrum is identical to the spectra published earlier for γ-irradiated samples[8] and is shown as the solid line in Figure 3a. The rate of formation of $\mathbf{6}^{\bullet+}$ obeys first-order kinetics (as measured from the growth in the amplitude of the central line, cf. Figure 3a), the rate constant depending on the temperature (Figure 4). Similar rate constants are found at 77 K in the $CFCl_2CF_2Cl$ matrix, and identical results are also obtained in parallel studies on allylamine deuterated at the NH_2 group. Significantly, the total spin concentration does not change during the transformation, indicating a 1:1 conversion of the primary radical cation $\mathbf{5}^{\bullet+}$ into the distonic species $\mathbf{6}^{\bullet+}$.

An apparent activation energy of 5.9 kJ mol^{-1} can be derived (Figure 4, inset) from the kinetic measurements in the investi-

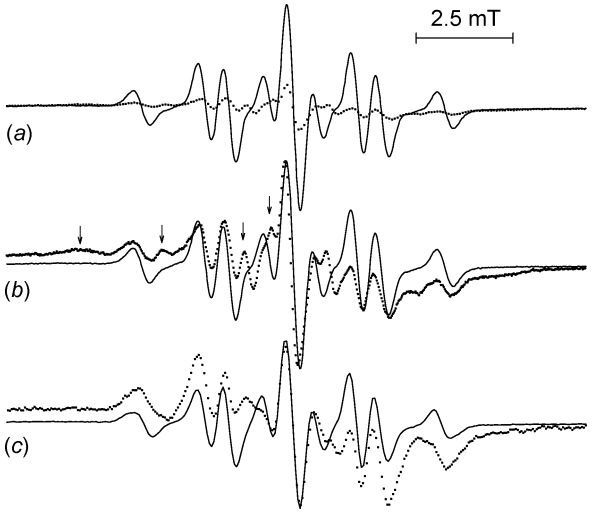

Figure 3. EPR spectra of frozen solutions (1:500) of allylamine (a and b) and allylamine-d_2 (c) in CF_3CCl_3, irradiated and measured at 77 K. Measurements were taken 2 (dotted) and 120 min (solid-line) after irradiation. Spectra in b and c are normalized at the central line for better comparison. The weak initial signals attributable to the primary radical cation $\mathbf{5}^{\bullet+}$ are indicated on the low-field side of spectrum b by vertical arrows.

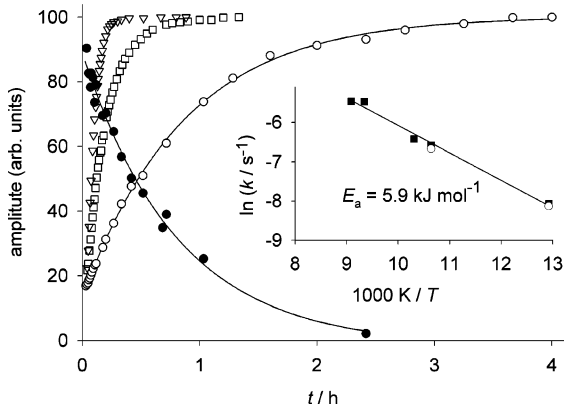

Figure 4. Kinetics of the formation of the iminopropyl radical cation $\mathbf{6}^{\bullet+}$ in the CF_3CCl_3 matrix, at *T*/K: 77 (○), 94 (□), and 107 (▽) and of the concomitant decay of the primary allylamine radical cation $\mathbf{5}^{\bullet+}$ at 77 K (●). Inset: Arrhenius plot for the apparent activation energy, data correspond to allylamine (■) and allylamine-d_2 (○).

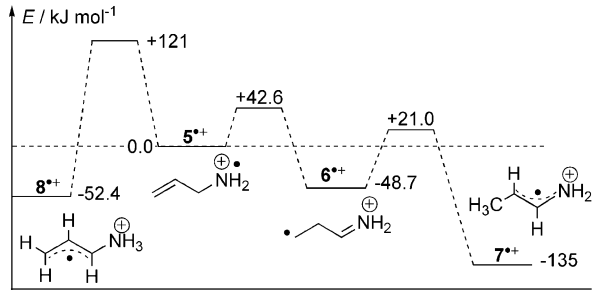

Figure 5. Energy diagram $\Delta(E_0 + \mathrm{ZPE})$ of transformations of the allylamine radical cation, calculated with B3LYP/6-31G(d,p).

gated temperature range (77−107 K). This is considerably lower than the calculated barrier height of ca. 43 kJ mol^{-1} (Figure 5), a value that is typical of H-atom transfer reactions[16] and which corresponds to the observed activation energy for such reactions in the gas phase at much higher temperatures.[16,17] However, as discussed in the previous paper on H-atom transfer in *n*-alkylamine radical cations,[5] this difference is understandable since quantum tunneling is likely to contribute to the reaction rate at cryogenic temperatures, and thus the apparent activation energy measured over a narrow temperature interval can be much less than the true barrier height.[16,17]

Even under our experimental conditions of rapid detection, the spectrum of the primary cation $\mathbf{5}^{\bullet+}$ turns out to be rather featureless at 77 K. This can be mainly attributed to a large anisotropy of the coupling constants for both nitrogen and the amine hydrogens, leading to a broadened spectrum that is overlapped by the much sharper lines from species $\mathbf{6}^{\bullet+}$. Nonetheless, even this broad anisotropic envelope from $\mathbf{5}^{\bullet+}$ can represent a significant spin concentration, as may be appreciated by comparing, for example, the reversible change between the broad and resolved patterns in the PAA spectra from $\mathbf{1}^{\bullet+}$ at 77 and 143 K (cf. Figure 1a,b).

Although the precise EPR characterization of $\mathbf{5}^{\bullet+}$ at 77 K is difficult, a closer inspection of the very first (2 min, dotted) and final (2 h, full line) spectra at 77 K, when normalized at the central line (Figure 3b), gives some hints as to the main features of the primary species. The EPR lines marked with an arrow in Figure 3b (only the low-field side is marked) disappear during the formation of species $\mathbf{6}^{\bullet+}$, and the rate constant for the decay of the noisy outermost line (marked with an arrow in Figure 3b) agrees reasonably well with that determined for the formation of $\mathbf{6}^{\bullet+}$ (cf. Figure 4 inset, 1.21 h^{-1} (●) and 1.15 h^{-1} (○) at 77 K, respectively). Furthermore, by comparing the very first recorded spectra for the allylamine and the *N*,*N*-dideuterioallylamine (dotted spectra in Figure 3b,c, respectively), the outermost lines in the former are not observed in the latter, clearly pointing to the replacement of larger $a(H_N)$ coupling constants by the corresponding smaller $a(D_N)$ ones. As in the cases of the propyl-[5] and propargyl-amines (Tables 1 and 2), this observation for species $\mathbf{5}^{\bullet+}$ is in line with quantum chemical calculations which predict that most of the spin density resides at nitrogen (Tables 3 and 4).

It is also noticeable that an initial steel-blue color disappears during the transformation, similar to the change observed in the photobleaching of PAA (vide infra). Quantum chemical calculations (UTD/B3LYP/6-311+G(d, p)) of optical absorption spectra predict that strong absorption bands in the 534−728 nm region (cf. Table 3) are only present for the primary species $\mathbf{5}^{\bullet+}$, which accounts for the observed (complementary) blue color. Therefore, the color change clearly supports the conclusion that the reaction involves the transformation of the primary radical cation $\mathbf{5}^{\bullet+}$.

In summary, we tentatively assign those weak lines marked with an arrow in Figure 3b to the primary radical cation $\mathbf{5}^{\bullet+}$ of allylamine. In contrast to the primary PAA species $\mathbf{1}^{\bullet+}$, the total spectral width of $\mathbf{5}^{\bullet+}$ is only ∼11 mT and, therefore, much less than the value observed for $\mathbf{1}^{\bullet+}$ (27 mT). As the calculated spin density distributions are quite comparable for both species, this discrepancy can only be explained by assuming smaller β-proton couplings for $\mathbf{5}^{\bullet+}$. This would in turn entail different geometrical conformations for $\mathbf{1}^{\bullet+}$ and $\mathbf{5}^{\bullet+}$ at the NH_2-CH_2 bond resulting from the interaction of the nitrogen p orbital with respect to the neighboring methylene group. This explanation is indeed supported by the calculation of the relative stabilities of the different conformers. In the case of PAA, the conformer $\mathbf{1b}^{\bullet+}$ (showing large H_β hfc's) is favored over $\mathbf{1a}^{\bullet+}$ by ∼4 kJ mol^{-1} (Table 1), whereas in the case of allylamine, the conformer $\mathbf{5a}^{\bullet+}$ (with the smaller H_β hfc's) is preferred over $\mathbf{5b}^{\bullet+}$ by ∼5 kJ mol^{-1}.

Allylamine−Photobleaching Experiments. To check on the stability of the radical cations $\mathbf{5}^{\bullet+}$ and $\mathbf{6}^{\bullet+}$ toward excitation by light, photobleaching experiments were performed. On account

TABLE 3: Spin Density (ρ), Mulliken Charge Distribution (q), and Coupling Constants a/mT for the Allylamine Radical Cation $5^{\bullet+}$, Its Isomers, and the Methyl Derivatives $9^{\bullet+}$ and $11^{\bullet+}$, Calculated with B3LYP/6-31G(d,p)[a]

	5a$^{\bullet+}$	**5b**$^{\bullet+}$	**6**$^{\bullet+}$	**7**$^{\bullet+}$	**8**$^{\bullet+}$	**9a**$^{\bullet+}$	**9b**$^{\bullet+}$	**11a**$^{\bullet+}$	**11b**$^{\bullet+}$
						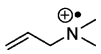		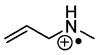	
$\Delta E(E_0+ZP)$		+5.04	-48.7	-135.2	-52.4		+0.89		+4.41
ρ(N)	**0.645**	**0.598**	0.093	**0.348**	-0.030	**0.805**	**0.812**	**0.744**	**0.797**
ρ(C1)	-0.004	-0.019	0.106	0.060	**0.609**	-0.034	-0.038	-0.021	-0.029
ρ(C2)	0.070	0.063	-0.066	**0.600**	-0.231	0.042	0.004	0.052	0.011
ρ(C3)	0.346	0.206	**0.923**	-0.036	**0.706**	0.046	0.017	0.166	0.052
ρ $(CH_3)_{av}$						-0.039	-0.040	-0.032	-0.027
q(N)	0.317	0.285	0.255	0.242	0.570	-0.202	-0.222	0.059	0.070
q(C1)	0.298	0.389	0.419	0.394	0.184	0.227	0.279	0.258	0.299
q(C2)	0.149	0.134	0.130	0.174	0.105	0.095	0.063	0.110	0.082
q(C3)	0.236	0.192	0.196	0.190	0.141	0.114	0.109	0.169	0.131
$q(CH_3)_{av}$						0.383	0.385	0.403	0.418
a(N)[b]	3.15/0.06	2.88/0.02	0.22/0.16	1.78/0.11	0.22/0.19	4.37/0.48	4.24/0.59	3.81/0.25	4.08/0.36
	1.09	(1.08)	(0.18)	(0.67)	(-0.20)	(1.78)	(1.81)	(1.44)	(1.61)
a(H,N)	-1.65 (2H)	-1.55 (2H)	-0.16/-0.23	-0.99 (2H)	1.12 (3H)	-	-	-1.93	-2.13
a(H,C1)	0.17/0.33	8.89/11.0	-0.25	-0.23	-1.58	2.59/0.04	5.51/2.92	1.59/0.01	7.07/3.46
a(H,C2)	0.03	-0.22	1.25/1.84	-1.46	0.42	0.072	0.13	0.13	0.20
a(H,C3)	-0.59/-0.37	-0.47/-0.50	-2.20 (2H)	2.46 (3H)	-1.64/-1.73	-0.03/0.19	-0.04 (2H)	-0.21/0.08	-0.12/-0.12
a(H,CH_3)						2.71 (6H)	2.73 (6H)	2.98 (3H)	3.43 (3H)
λ/nm	534 (0.076)	748 (0.083)	380 (0.085)	275 (0.016)	315 (0.006)	698 (0.019)	692 (0.013)	794 (0.034)	905 (0.021)
	301 (0.021)	294 (0.005)	231 (0.028)	228 (0.326)	215 (0.316)	301 (0.040)	310 (0.005)	340 (0.015)	350 (0.007)

[a] Data are given for the most stable conformer. Relative stability ΔE/kJ mol^{-1} (including zero-point vibrational energy) is calculated with respect to the most stable primary species. Wavelengths λ/nm (calculated with B3LYP/6-311+G(d,p)) correspond to the transitions with lowest energy showing significant intensity (oscillator strength given in brackets). [b] Anisotropy for nitrogen coupling is given as $a_{||}/a_{\perp}$; a_{iso} (given in brackets) = 1/3 ($a_{||}$ + 2$a_{\perp}$).

TABLE 4: Calculated with BH&HLYP/6-31G(d,p)[a]

	5a$^{\bullet+}$	**5b**$^{\bullet+}$	**6**$^{\bullet+}$	**7**$^{\bullet+}$	**8**$^{\bullet+}$	**9a**$^{\bullet+}$	**9b**$^{\bullet+}$	**11a**$^{\bullet+}$	**11b**$^{\bullet+}$
ΔE (E_0 + ZP)		+15.1	−61.8	−144.0	−66.7		+1.13		+1.67
ρ(N)	**0.713**	**0.824**	0.058	**0.366**	−0.040	**0.807**	**0.908**	**0.886**	**0.925**
ρ(C1)	−0.008	−0.051	0.061	0.003	**0.683**	−0.057	−0.063	−0.043	−0.057
ρ(C2)	0.037	−0.006	−0.084	**0.672**	−0.358	0.030	0.007	0.007	0.009
ρ(C3)	0.408	0.100	**1.037**	−0.058	**0.781**	0.024	0.002	0.117	0.008
$\rho(CH_3)_{av}$						−0.063	−0.063	−0.061	−0.057
q(N)	0.336	0.359	0.246	0.230	0.568	−0.234	−0.255	0.087	0.087
q(C1)	0.315	0.388	0.485	0.424	0.199	0.248	0.297	0.266	0.299
q(C2)	0.120	0.067	0.107	0.166	0.092	0.072	0.063	0.073	0.056
q(C3)	0.229	0.149	0.161	0.179	0.140	0.112	0.041	0.149	0.125
$q(CH_3)_{av}$						0.401	0.112	0.425	0.432
$a(N)_{iso}$[b]	3.64/0.43	4.18/0.74	0.34/0.05	2.08/0.35	−0.26/−0.24	5.27/1.04	5.12/1.11	4.85/0.76	5.10/0.91
	(1.50)	(1.89)	(0.15)	(0.93)	(−0.25)	(2.45)	(2.48)	(2.14)	(2.32)
a(H,N)	−2.16 (2H)	2.49 (2H)	−0.10/−0.17	−1.25 (2H)	1.20 (3H)			−2.64	−2.81
a(H,C1)	0.28/0.11	9.62 (2H)	−0.14	−0.10	−2.02	3.05/0.07	5.07/3.02	2.09/0.10	6.56/2.38
a(H,C2)	0.15	−0.07	1.43/1.61	−1.76	0.77	−0.02	0.13	0.11	0.10
a(H,C3)	−0.89/−0.75	−0.25/−0.28	−2.72 (2H)	2.34 (3H)	−1.98/−2.09	−0.03/0.10	0.01/0.00	−0.20/0.03	−0.02/−0.03
a(H,CH_3)						2.75 (6H)	2.73 (6H)	3.16 (3H)	3.42 (3H)

[a] For details, see Table 3. [b] Anisotropy for nitrogen coupling is given as $a_{||}/a_{\perp}$; a_{iso} (given in brackets) = 1/3 ($a_{||}$ + 2$a_{\perp}$).

of the short lifetime of $5^{\bullet+}$, the sample was exposed to visible light during the e-beam irradiation. Although only the same distonic species $6^{\bullet+}$ is produced under these conditions, it is now completely formed after a few minutes. The fact that light significantly enhances the rate of transformation can readily explain the otherwise curious observation that 20% of the distonic species is observed after the first minute of irradiation, whereas its further formation after removal from the e-beam proceeds at a much slower rate with a half-life of ∼1 h (cf. Figure 4). Accordingly, it is highly probable that the Cerenkov and luminescence light inherently produced by the high-energy irradiation serves to accelerate the transformation of $5^{\bullet+}$ to $6^{\bullet+}$.

Whereas the distonic species $6^{\bullet+}$ is quite stable to visible light, it undergoes a slow photobleaching with UV light ($\lambda \sim 350$ nm) to yield the final spectrum shown in Figure 6a (solid black line). If one assumes that a further intramolecular rearrangement takes place, the most likely product is the 1-aminopropene radical cation $7^{\bullet+}$ resulting from a 2,3-H shift (Scheme 5), and calculations show that this $CH_3CH{=}CHNH_2^{\bullet+}$ species is the most stable $C_3H_7N^{\bullet+}$ isomer. Moreover, in mass spectrometric work on the gas-phase transformations of $C_3H_7N^{\bullet+}$ isomers, $7^{\bullet+}$ has been identified as the end product in the sequence of reactions originating from the cyclopropylamine radical cation.[7b,d] Indeed, a satisfying fit (Figure 6a, gray line) can be obtained to the final photobleached spectrum (Figure 6a, solid black line) using the coupling constants a/mT of 2.35 (3H), 1.6 (1H), 0.98 ($2H_N$), and 1.15/0.65 (1N, $a_{||}/a_{\perp}$) in close agreement with the calculated values for $7^{\bullet+}$ (see Tables 3 and 4).

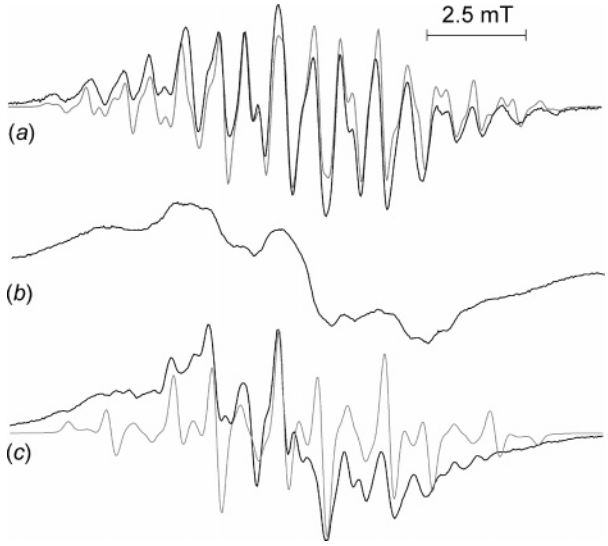

Figure 6. EPR spectra observed after photobleaching of frozen solutions (1:500) of allylamine (a) and allylamine-d_2 (b and c) in CF_3CCl_3, irradiated at 77 K and measured at 95 K (b) and 130 K (a and c). Simulation given as gray lines (for hfc see text).

SCHEME 2

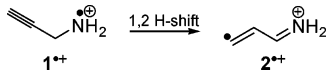

SCHEME 3

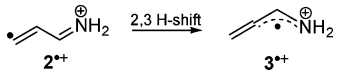

SCHEME 4

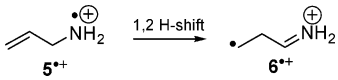

SCHEME 5

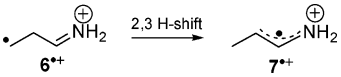

SCHEME 6

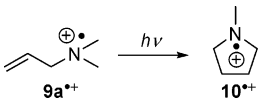

Further proof of this assignment is established by a similar experiment with partially deuterated allylamine, in which illumination of the distonic radical cation **6**$^{\bullet+}$ derived from *N*,*N*-dideuterioallylamine with UV-light at 95 K leads to the broad, structureless spectrum shown in Figure 6b which then transforms reversibly at 130 K into the better resolved spectrum in Figure 6c (solid black line). It can be seen that relative to the spectrum in Figure 6a obtained from the undeuterated allylamine, the spectral width in Figure 6c is slightly reduced as would be expected for the replacement of a 1:2:1 triplet with $a(2H_N)$ of ~1 mT (from the two amino-protons) by a 1:2:3:2:1 quintet with the smaller coupling $a(2D_N)$ of ~ 0.16 mT (from the two amino-deuterons). This spectral narrowing is even more apparent since the quintet remains unresolved because of the large line width (ca. 0.3−0.5 mT) under these frozen matrix conditions. Simulating the spectrum of species $CH_3CH{=}CHND_2^{\bullet+}$ (7-$D_2^{\bullet+}$) with coupling constants *a*/mT of 2.66 (3H), 1.68 (1H) and 1.05/0.35 (1N, $a_{\parallel}/a_{\perp}$), quite comparable to those of 7-$H_2^{\bullet+}$, and taking the contribution of the amino-deuterons into account through a slightly increased line width, all main features are reproduced well as shown in Figure 6c (gray line). The slight increase in these apparent values for the hydrogen couplings in 7-$D_2^{\bullet+}$ as compared to 7-$H_2^{\bullet+}$ may also be a reflection of the unresolved deuterium couplings, the effect serving in this case to augment the much larger hydrogen values.

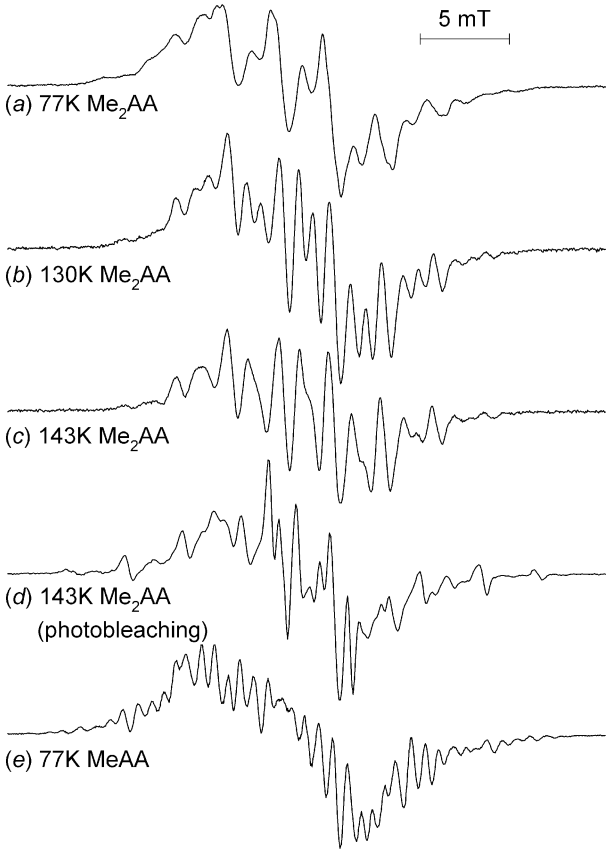

Figure 7. EPR spectra of frozen solutions (1:500) of dimethyl allylamine (a−c) and methylallylamine (e) in CF_3CCl_3, irradiated at 77 K and measured at the temperatures indicated. (d) obtained after photobleaching.

***N*,*N*-Dimethylallylamine and *N*-Methylallylamine.** Experiments on these substituted allylamines were performed in order to see if the replacement of the amino hydrogens by electron donating groups has any influence on the stability of the primary radical cation with regard to the spontaneous 1,2-H shift that occurs for the parent allylamine species. The spectrum observed in the case of dimethylallylamine (Me_2AA) in CF_3CCl_3 at 77 K in the dark is shown in Figure 7a. Increasing the temperature to 130 and 143 K (Figure 7b,c) leads to progressively improved resolution and an interesting change in the line pattern which is, however, completely reversible. The position of the sharpest set of lines does not change significantly (cf. Figure 7a−c), and, to a good approximation, these lines appear to constitute a binomial octet with a splitting of 2.8−3.0 mT. Such a pattern is compatible only with an assignment to the primary radical cation **9a**$^{\bullet+}$ with 6 equiv methyl protons and only one additional β-proton since none of the other isomers can provide an adequate number of strongly coupled equivalent nuclei. The insensitivity of the octet pattern to temperature, especially in regard to the splitting represented by the prominent central doublet (as determined by the unique β proton), establishes that the observed changes in the intervening lines of the spectrum are not due to a conformational effect.[18] Therefore, the most likely explanation for the temperature dependence is the partial

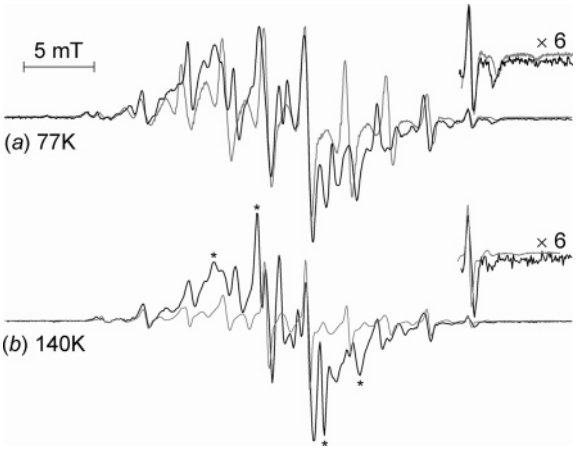

Figure 8. EPR spectra of frozen solutions (1:500) of dimethylallylamine after photobleaching (black line) and *N*-methylpyrrolidine (gray line) in CF_3CCl_3, irradiated at 77 K and measured at the temperatures indicated. Signals attributable mainly to a second species (probably a neutral radical) are marked with an asterisk.

dynamical averaging of the anisotropic nitrogen coupling. Accordingly, keeping all proton hfc constants fixed at 2.85 mT (6H) and 3.1 mT (1H$_\beta$), satisfying simulations over the entire temperature range are obtained by using the following axially symmetric hfc tensor data for nitrogen as a function of temperature: $a_{||}/a_\perp$ = 4.3/0.2 mT (95 K), 3.3/1 mT (130 K), and 2.0/1.55 mT (143 K).

Upon photobleaching with UV light, a much wider spectrum is observed (Figure 7d) suggesting that several large β-hydrogen couplings contribute to the splitting pattern, which also indicates the presence of a methyl group (see sharp lines outside the central part). Additionally, small wing features attributable to anisotropic nitrogen couplings are observed (cf. Figure 8, magnified spectra) pointing to the presence of significant spin density at nitrogen. Since none of the linear isomers resulting from H-shifts similar to those observed for allylamine could give rise to both a large spectral extent and a methyl group splitting, the simplest explanation would be a conformational change of the dimethylamino group with respect to the rest of the molecule, leading to conformer **9b**$^{\bullet+}$. This conformer is calculated to have nearly the same energy (+1 kJ mol^{-1}) as **9a**$^{\bullet+}$ and is only separated from the latter by a rotational barrier of 6.75 kJ mol^{-1}. However, simulation of the spectrum would require a relative *g* shift of 0.0006 (ΔH = 0.1 mT) and a coupling constant of 3.2 mT (6H) for the methyl hydrogens, a value significantly larger than that for conformer **9a**$^{\bullet+}$ (2.85 mT (6H)). Both experimental findings make the assumption of a mere change to rotamer **9b**$^{\bullet+}$ unlikely.

Having therefore ruled out a simple conformational change as well as the formation of linear isomeric radical cations resulting from hydrogen shifts in the carbon chain, we now present experimental results that strongly support the remarkable and unexpected formation of the 1-methylpyrrolidine radical cation **10**$^{\bullet+}$ from **9a**$^{\bullet+}$ (Scheme 6).

The evidence comes from a comparison of the photobleached spectra with the corresponding spectra of the 1-methylpyrrolidine radical cation derived directly from its parent compound (cf. Figure 8). Except for some additional lines found in the central part of the spectrum (probably attributable to a neutral radical, which could not be assigned), the spectra agree quite well, even at different temperatures (i.e., they show the same change in the anisotropy of N) and the derived EPR parameters *a*/mT (29.5(3H), 56.1 (2H), 30 (2H), and 39/9 (1N, $a_{||}/a_\perp$)) are in excellent agreement with those reported by Shiotani et al.[19]

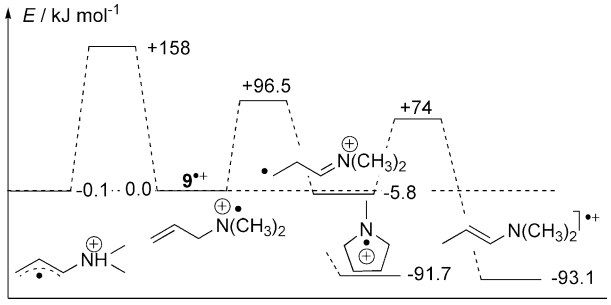

Figure 9. Energy diagram $\Delta(E_0 + \text{ZPE})$ of transformations of the *N*,*N*-dimethylallylamine radical cation, calculated with B3LYP/6-31G(d,p).

(29.4(3H), 57.3 (2H), 28.5 (2H), and 40/5 (1N, $a_{||}/a_\perp$)). The small differences in the β-proton couplings (and thus of the position of the inner lines) are rationalized in terms of slightly different geometries of the radical cations derived from either the "relaxed" parent molecule (1-methyl pyrrolidine) or via the extensive bond rearrangement that takes place in the photoinduced cyclization of $Me_2AA^{\bullet+}$. As discussed later on, the reaction can be represented as a concerted H-atom transfer from one of the aminomethyl groups to the internal (C2) carbon at the double bond followed by intramolecular radical addition at the $CH_2{=}N^+(Me)R$ group to bring about the subsequent ring closure. The overall reaction is exothermic by −91.7 kJ/mol (B3LYP, cf. Figure 9).

Turning now to *N*-methylallylamine (MeAA), the initial spectrum observed in CF_3CCl_3 after irradiation at 77 K in the dark is shown in Figure 7e. On increasing the temperature to 143 K, a small reversible change occurs in the line pattern that can again be explained by the partial averaging of the anisotropic nitrogen coupling. A good approximation for this spectrum is obtained using a set of coupling constants derived from the calculated data for the primary radical cation **11b**$^{\bullet+}$ with two large β-proton couplings. Although a slightly higher energy is calculated (in vacuo) for this conformer in comparison with conformer **11a**$^{\bullet+}$, the former may be preferred due to its smaller (spherical) size providing for a better fit into matrix cavities.

In contrast to the striking results described for the photobleaching of the Me_2AA radical cation **9a**$^{\bullet+}$, the MeAA radical cation **11b**$^{\bullet+}$ is stable upon illumination with UV-light ($\lambda \geq$ 350 nm). This is surprising since the calculated absorption bands in Table 3 for **11b**$^{\bullet+}$ (350 and 850 nm) lie at slightly longer wavelengths than those of **9a**$^{\bullet+}$ (300 and 700 nm) and are therefore similarly available for UV/visible excitation. Also, although the calculated exothermicity for the corresponding cyclization of **11b**$^{\bullet+}$ (−72 kJ/mol) is slightly less than that (−91.7 kJ/mol) for **9a**$^{\bullet+}$, there is still a considerable driving force for a potential reaction. Thus, the failure to bring about the photoinduced cyclization of the MeAA radical cation **11b**$^{\bullet+}$ suggests that in its excited state either a significant barrier or a rapid internal conversion process prevents it from undergoing the rather extensive rearrangement process (vide infra) needed for the transformation. Evidently, the extra methyl group in the Me_2AA radical cation is critical to the reaction, perhaps through the stabilization of the nitrogen-centered cation that persists throughout the H-atom shift and subsequent cyclization.

Discussion

Structure and Stability of Isomeric Radical Cations. The experimental results clearly highlight the basic similarity of the parent propargylamine and allylamine cations with respect to their primarily nitrogen-centered radical structures. Also, analo-

gous results were recently obtained with 3-pyrroline (2,5-dihydropyrrole, 2,5-DHP),[20] a congeneric molecule with a similar $N-C-C_{unsaturated}$ backbone although it is geometrically constrained due to the ring structure. For all three primary radical cations, about two-thirds of the total spin density is calculated to be localized on nitrogen (0.645, 0.686, and 0.689 for AA, PAA, and 2,5-DHP, respectively), which is consistent with the very similar range of experimental values of the hfs coupling constants for the amino proton(s) and for nitrogen ($a(H_N) \approx 1.55-1.87$ mT and $a(N)_{iso} \approx 1.1-1.4$ mT) in these primary species. Moreover, the conformational geometry at the amine moiety of the propargylamine radical cation **1b**$^{\bullet+}$ resembles that of 2,5-DHP$^{\bullet+}$,[20] as large β-proton couplings of $\sim$7 mT were observed in both cases.

Recalling the observations that the primary radical cations **1b**$^{\bullet+}$, **5a**$^{\bullet+}$, and 2,5-DHP$^{\bullet+}$ all are blue after irradiation and that the blue color disappears during transformation, it is pertinent to consider the nature of the underlying optical transition in more detail. The calculations show in each case (this is true also for the radical cations of the methylated allylamine derivatives) that the transition in the (infra)red spectral range is due to an intramolecular electron transfer from the π orbital on the vinyl group to the n orbital on nitrogen. This transfer results in a shift of the spin density in the excited radical cations from nitrogen to the vinyl double bond, facilitating the subsequent H atom transfer by the 1,2 H-shift in the case of **1b**$^{\bullet+}$, **5a**$^{\bullet+}$, and 2,5-DHP$^{\bullet+}$ or the 1,4 H-shift via a five-membered ring transition state in the case of Me_2AA (**9a**$^{\bullet+}$).

A close parallelism also exists with respect to the daughter isomers produced by the analogous sequence of subsequent intramolecular H-shifts. Concerning the initial rearrangements of the parent cations to their distonic species, it is insightful to consider the mechanism by which this 1,2-hydrogen shift takes place from the saturated α-CH_2 group to the unsaturated β-carbon. Although it should be stressed that the actual H-shift is almost certainly concerted, it can be represented as occurring in two distinct steps, involving both H-atom elimination and readdition. First, the H-atom is removed from the neighboring carbon of the nitrogen-centered parent cation in what is essentially a β-elimination reaction with the resulting formation of a π bond between the positively charged nitrogen and the adjacent carbon atom. Although this first step would be endothermic if considered in isolation because of the H-atom dissociation, the concomitant π-bond formation at nitrogen certainly provides part of the driving force for the overall reaction, irrespective of whether it occurs thermally (as in AA) or photochemically (as in PAA and 2,5-DHP[20]). A similar type of oxygen-carbon π bonding occurs as a result of the corresponding H-atom shift in the thermal rearrangement of the oxygen-centered 2,5-dihydrofuran radical cation to the distonic carbon-centered 2,4-dihydrofuran species.[9a] Thus, in each case, part of the potential reactivity of the parent radical cation can be attributed to the tendency for the ionized "tetravalent" nitrogen or "trivalent" oxygen to complete its valence shell of electrons through the formation of this additional π bonding.[21] The second step in the overall reaction occurs by the exothermic readdition of the "eliminated" H-atom to the alkene or alkyne group, thereby generating a carbon-centered radical that is separated from the positively charged nitrogen or oxygen cation. The distonic radical cations **2**$^{\bullet+}$, **6**$^{\bullet+}$, and 2,4-DHP$^{\bullet+}$ that are formed do not have a neutral biradical counterpart but are calculated to be more stable than their isomers **1**$^{\bullet+}$, **5**$^{\bullet+}$, and 2,5-DHP$^{\bullet+}$ derived directly by radiolytic oxidation of the parent compounds.

The primary radical cation **5**$^{\bullet+}$ of AA is unstable even at 77 K and transforms spontaneously by first-order kinetics into the iminopropyl radical cation **6**$^{\bullet+}$ with a half-life ($t_{1/2}$) of less than 1 h. The greater ease of transformation in the case of AA can obviously be explained by the much lower activation barrier of 43 kJ mol^{-1} as compared with PAA and 2,5-DHP (61 and 90 kJ mol^{-1}, respectively). For these higher barriers, some form of additional excitation (e.g., by light) is generally needed to drive the reaction, and we find that a similar H-transfer is readily induced by low-energy ($\lambda > 600$ nm) light in the cases of PAA and 2,5-DHP.[20] The thermal rearrangement of **5**$^{\bullet+}$ to **6**$^{\bullet+}$ is quite analogous to the transformation of the oxygen-centered 2,5-dihydrofuran radical cation to the distonic carbon-centered 2,4-dihydrofuran species and occurs on a comparable time scale.[9a]

The fact that the apparent Arrhenius activation energy (5.9 kJ mol^{-1}, Figure 4) derived from the kinetic studies over the narrow temperature range of 77−107 K is much lower than the barrier height predicted theoretically (ca. 43 kJ mol^{-1}) strongly suggests that a large contribution from quantum mechanical tunneling becomes significant for H-atom transfer under these cryogenic conditions.[16] A similar "discrepancy" between calculated and measured activation energies was also observed for the 1,5 H-shifts of ionized *n*-propylamine (10.8 vs 71.6 kJ mol^{-1}, respectively)[5] and methylacrylate (4.5 vs 57.6 kJ mol^{-1}),[9b] pointing to a more general effect in these frozen Freon matrices. As a tentative practical guideline, it appears that such spontaneous intramolecular H-atom transformations can occur in the temperature range of 77−145 K if the calculated activation energy lies below $\sim$80 kJ mol^{-1}. It may be experimentally accessible ($t_{1/2} \geq 5$ min) with conventional EPR and e-beam methodology provided the calculated barrier is larger than $\sim$30 kJ mol^{-1}; otherwise, even at 77 K, the reaction occurs too rapidly (e.g., as in the case of *n*-butylamine[5] for which the barrier for H-shift was calculated to be 13.5 kJ mol^{-1}) to be followed by the present technique. For barriers significantly larger than 80 kJ mol^{-1}, however, the contribution of tunneling seems to be less significant, probably on account of a corresponding increase in the barrier width, and the spontaneous rearrangement does not occur.

Further photoinduced transformations ($350 < \lambda < 600$ nm) of **2**$^{\bullet+}$, **6**$^{\bullet+}$, and 2,4-DHP$^{\bullet+}$ lead respectively to the most stable isomers **3**$^{\bullet+}$, **7**$^{\bullet+}$, and 2,3-DHP$^{\bullet+}$,[20] which are all characterized by a resonance-stabilized hetero-allylic radical structure. According to the calculations in Tables 1−4, the unsymmetrical structures of **3**$^{\bullet+}$ and **7**$^{\bullet+}$ are both characterized by a larger spin density on the C2 carbon (0.57−0.67) than on the nitrogen (0.35−0.42). A similar result is found for 2,3-DHP$^{\bullet+}$,[20] and there is excellent agreement between the calculated and experimental hyperfine coupling constants for all three species.

Although previous mass spectrometric[7b] and associated computational studies[7d] have described the conversion of **6**$^{\bullet+}$ to **7**$^{\bullet+}$ in the gas phase, the present work provides the first observation of the reaction under matrix conditions. In this connection, the interesting point has been raised[7d] as to why the spontaneous thermal transformation of both the cyclopropylamine radical cation and **5**$^{\bullet+}$ proceed only as far as **6**$^{\bullet+}$ in a matrix[7a,8] whereas the end product in the gas phase[7b] is the more stable **7**$^{\bullet+}$, as would be expected for a barrier-less series of transformations from the initial high-energy species. The answer undoubtedly lies in the ability of the matrix to rapidly quench any excess energy with which **6**$^{\bullet+}$ is formed; consequently, a barrier is introduced preventing its further transformation to **7**$^{\bullet+}$.

Although unexpected, the photoconversion of the dimethylallylamine (Me_2AA) radical cation **9a**$^{\bullet+}$ to the 1-methylpyrrolidine radical cation **10**$^{\bullet+}$ can be rationalized in terms of the formation of a precursor species that precedes the cyclization. This can occur by a modified H-atom shift mechanism with the basic motifs being essentially similar to those already described for the rearrangement of the other primary radical cations **1**$^{\bullet+}$, **5**$^{\bullet+}$, and 2,5-DHP$^{\bullet+}$. For the Me_2AA radical cation, the only difference is that the first step in the analysis now involves the removal of the H-atom from one of the methyl groups rather than from the α-CH_2 of the allylic group. Then, in the completely analogous second step, this H-atom adds to the penultimate carbon of the allylic moiety so as to generate the corresponding distonic radical cation $MeN^+(=CH_2)CH_2$-$CH_2CH_2^{\bullet}$ which is thereby poised to undergo the subsequent cyclization to the 1-methylpyrrolidine radical cation **10**$^{\bullet+}$. In the actual reaction, of course, the transfer of the H-atom from the methyl group to the penultimate allylic carbon is likely to be highly concerted through the formation of a five-membered transition state. Furthermore, since the positive charge remains on nitrogen throughout the sequence, it is also possible that the entire reaction is concerted in the sense that the radical addition leading to cyclization is already partly underway before the H-atom transfer is completed. The fact that the allylamine distonic radical cation **6**$^{\bullet+}$ fails to undergo a similar kind of cyclization to the cyclopropylamine radical cation can obviously be attributed to the larger ring-strain energy of cyclopropane relative to that of the five-membered pyrrolidine structure. Indeed, as already mentioned in the Introduction, it is the reverse process that is found in which the parent cyclopropylamine radical cation spontaneously rearranges to **6**$^{\bullet+}$.[7a,b,d]

When considered in terms of the constituent steps of H-atom transfer and cycloaddition, the photoconversion of **9a**$^{\bullet+}$ to **10**$^{\bullet+}$ formally resembles the thermal rearrangements by which the ethyl acrylate (EtA) radical cation[9b] is transformed into cyclic species. Thus, an H-atom transfer occurs spontaneously at low temperature in EtA$^{\bullet+}$ from the terminus of the ethyl group to the ionized oxygen atom of the C=O group, and this is followed at higher temperature by the internal addition of the $CH_2^{\bullet}$ radical center to the vinyl group. Depending on the mode of cycloaddition at the vinyl double bond, either a five- or six-membered ring structure is thereby formed.[9b] However, the resulting cyclized radical cations from EtA are carbon-centered radicals rather than oxygen-centered radical cations analogous to the nitrogen center in **10**$^{\bullet+}$. Moreover, in contrast to the 1-methylpyrrolidine radical cation where the nitrogen atom is incorporated in the five-membered ring, the original ionized oxygen atom in EtA$^{\bullet+}$ finishes up in each case as a substituent OH group in the two cyclic species.[9b]

Conclusion

This work demonstrates the remarkably facile nature of H-atom transfer processes in the unimolecular rearrangements of unsaturated amine radical cations studied by matrix isolation at low temperatures. The parent propargylamine (PAA) and allylamine (AA) radical cations both undergo consecutive H-atom shifts to generate intrinsically more stable isomers. For PAA, the transformation of the parent **1b**$^{\bullet+}$ species to the vinyl-type distonic radical cation **2**$^{\bullet+}$ is induced by visible light, whereas the further conversion of the latter to the allene-type heteroallylic species **3**$^{\bullet+}$ is brought about by UV excitation. In the case of AA, however, the first step by which the parent species **5a**$^{\bullet+}$ undergoes a 1,2-H-atom shift to generate the alkyl-type distonic radical cation **6**$^{\bullet+}$ can also occur directly at low temperatures with an activation energy that is much less than the calculated barrier height, which is suggestive of a large contribution from quantum tunneling. Since the rate of this **5a**$^{\bullet+}$ $\rightarrow$ **6**$^{\bullet+}$ reaction can be accelerated by exposure to visible light, the parent AA species **5a**$^{\bullet+}$ like that of PAA **1b**$^{\bullet+}$ possesses a reactive chromophore that is identified in each case with a blue color. The subsequent conversion of **6**$^{\bullet+}$ to the more stable 1-aminopropene species **7**$^{\bullet+}$ requires photoexcitation with UV light, paralleling the conditions for the corresponding **2**$^{\bullet+}$ $\rightarrow$ **3**$^{\bullet+}$ isomerization in the PAA series.

Insight into the mechanism of the first photochemical step in both the PAA and AA series is provided by quantum chemical calculations. These show that the excited states produced by the optical transitions in the visible to near-IR region for the parent PAA **1b**$^{\bullet+}$ and AA **5a**$^{\bullet+}$ species result in an intramolecular electron transfer from the π-orbital of the unsaturated group to the ionized lone-pair *n*-orbital on nitrogen. As a result, the migration of the spin density from nitrogen to the propargyl or allyl region of the molecule helps to bring about the 1,2 H-shift resulting in the formation of the distonic species **2**$^{\bullet+}$ and **6**$^{\bullet+}$ from **1b**$^{\bullet+}$ and **5a**$^{\bullet+}$, respectively. In the absence of photoexcitation, the 1,2 H-shift that converts **5a**$^{\bullet+}$ spontaneously to **6**$^{\bullet+}$ is likewise driven by the tendency for the ionized nitrogen to complete its valence shell of electrons through the formation of $-CH{=}NH_2^+$ π bonding[21] and spin density transfer to the terminal carbon of the allyl group.

An unexpected finding is the remarkable photochemical rearrangement of the dimethylallylamine (Me_2AA) radical cation **9a**$^{\bullet+}$ to the 1-methylpyrrolidine radical cation **10**$^{\bullet+}$. Although it might have been anticipated that the additional stability conferred on **9a**$^{\bullet+}$ by the presence of the two electron donating methyl groups on nitrogen would render the 1,2 H shift less likely than for the parent AA radical cation **1b**$^{\bullet+}$, the occurrence of this alternative reaction involving ring formation seems to be unprecedented. However, the overall reaction can be rationalized in terms of a modified H-atom shift mechanism in which the first step involves the migration of the H-atom from one of the methyl groups (rather than from the α-CH_2 of the allylic group) to produce a distonic radical cation similar to **6**$^{\bullet+}$. Ring closure can then readily occur in this $MeN^+(=CH_2)CH_2CH_2$-$CH_2^{\bullet}$ precursor species by the straightforward addition of the alkyl radical center to the carbon end of the newly formed iminium ion. In this way, the radical cation center is regenerated at the nitrogen atom. Hence, the overall transformation of the open Me_2AA radical cation **9a**$^{\bullet+}$ to the cyclic 1-methylpyrrolidine **10**$^{\bullet+}$ occurs with only a minor change in the substitution pattern ($-CH_2R$ for $-CH_3$) at the nitrogen radical cation. Clearly, the electronic driving force for this photoinduced cyclization originates with the intramolecular electron transfer in the excited-state of **9a**$^{\bullet+}$ which in turn drives the H-atom shift to generate the distonic radical cation precursor.

Acknowledgment. The authors are grateful to Professor Vladimir I. Feldman (Karpov Institute of Physical Chemistry, Moscow, Russia) for his helpful discussion of the radical reaction of the DiMeAA radical cation. One of us (F.W.) also thanks Steven J. Randolph for contributing to some preliminary EPR studies on these systems and for his interest in the problem.

References and Notes

(1) (a) Das, S.; Suresh, V. In *Electron Transfer in Chemistry*; Balzani V., Ed.; Wiley-VCH: Weinheim, 2001; Vol. II, Part 1, Chapter 7, pp 379−456. (b) Yoon, U. C.; Mariano, P. S.; Givens, R. S.; Atwater, B. W., III In *Advances in Electron Transfer Chemistry*; Mariano, P. S., Ed.; JAI Press Inc.: Greenwich, Connecticut, 1994; Vol. 4, pp 117−205.

(2) (a) Giese, B. *Radicals in Organic Synthesis: Formation of Carbon-Carbon Bonds*; Pergamon Press: New York, 1986. (b) Easton, C. J. *Chem. Rev.* **1997**, *97*, 53−82. (c) Lewis, F. D. In *Advances in Electron Transfer Chemistry*; Mariano P. S., Ed.; JAI Press Inc.: Greenwich, Connecticut, 1996; Vol. 5, pp 1−40. (d) Mattay, J. *Synthesis* **1989**, 233−252.

(3) (a) Stubbe, J.; van der Donk, W. A. *Chem. Rev.* **1998**, *98*, 705. (b) Guengerich, F. P.; McDonald, T. L. In *Advances in Electron Transfer Chemistry*; Mariano, P. S., Ed.; JAI Press Inc.: Greenwich, Connecticut, 1993; Vol. 3, pp 191−241. (c) Silverman, R. B. In *Advances in Electron Transfer Chemistry*; Mariano, P. S., Ed.; JAI Press Inc.: Greenwich, Connecticut, 1992; Vol. 2, pp 177−213. (d) Tullman, R. H.; Hanzlik, R. P. *Drug Metabolism Rev.* **1984**, *15*, 1163−1182. (e) Abeles, R. H.; Maycock, A. L. *Acc. Chem. Res.* **1976**, *9*, 313−319. (f) Maycock, A. L.; Abeles, R. H.; Salach, J. I.; Singer, T. P. *Biochemistry* **1976**, *15*, 114.

(4) (a) Steckhan, E. In *Organic Electrochemistry*; Lund, H., Baizer, M. M., Eds.; M. Dekker: New York, 1990; pp 581−613. (b) Theys, R. D.; Sosnovsky, G. *Chem. Rev.* **1997**, *97*, 83−132. (c) Novák, P.; Müller, K.; Santhanam, K. S. V.; Haas, O. *Chem. Rev.* **1997**, *97*, 1515−1566. (d) Kido, J.; Kimura, M.; Nagai, K. *Science* **1996**, *275*, 1267−1332.

(5) Janovský, I.; Knolle, W.; Naumov, S.; Williams, F. *Chem. Eur. J.* **2004**, *10*, 5524.

(6) Fally, F.; Doneux, C.; Riga, J.; Verbist, J. J. *J. Appl. Polym. Sci.* **1995**, *56*, 597−614.

(7) (a) Qin, X.-Z.; Williams, F. *J. Am. Chem. Soc.* **1987**, *109*, 595. (b) Bouchoux, G.; Alcaraz, C.; Dutuit, O.; Nguyen, M. T. *J. Am. Chem. Soc.* **1998**, *120*, 52. (c) Bouchoux, G.; Flament, J. P.; Hoppilliard, Y.; Tortajada, J.; Flamang, R.; Maquestiau, A. *J. Am. Chem. Soc.* **1989**, *111*, 5560. (d) Nguyen, M. T.; Creve, S.; Ha, T.-K. *Chem. Phys. Lett.* **1998**, *293*, 90.

(8) Dai, S.; Guo, Q.-X.; Wang, J. T.; Williams, F. *J. Chem. Soc. Chem. Commun.* **1988**, 1069.

(9) (a) Knolle, W.; Janovský, I.; Naumov, S.; Mehnert, R. *J. Chem. Soc., Perkin. Trans. 2* **1999**, 2447. (b) Knolle, W.; Feldman, V. I.; Janovský, I.; Naumov, S.; Mehnert, R.; Langguth, H.; Sukhov, F. F.; Orlov, A. Yu. *J. Chem. Soc., Perkin. Trans. 2* **2002**, 687. (c) An alternative method for the EPR detection of thermally labile radical cations is that of X-ray irradiation in situ at 4.2 K; see, for example: Iwasaki, M.; Toriyama, K.; Nunome, K. *J. Am. Chem. Soc.* **1981**, *103*, 3591. However, spectra measured at 4 K are often subject to additional line broadening and microwave power saturation effects due to long relaxation times, and the radical decay processes are generally inferred from annealing experiments carried out over a wide temperature range. In comparison, the e-beam method offers several distinct advantages through much shorter radiation exposures, better spectral resolution, and the ability to directly monitor the transformations by way of isothermal kinetics at conveniently chosen temperatures.

(10) Duling, D. R. *J. Magn. Reson. Ser. B* **1994**, *104*, 105.

(11) (a) Becke, A. D. *J. Chem. Phys.* **1993**, *98*, 5648. (b) Lee, C.; Yang, W.; Parr, R. G. *Phys. Rev. B* **1988**, *37*, 785; (c) Becke, A. D. *J. Chem. Phys.* **1996**, *104*, 1040.

(12) Frisch, M. J.; Trucks, G. W.; Schlegel, H. B.; Scuseria, G. E.; Robb, M. A.; Cheeseman, J. R.; Montgomery, J. A., Jr.; Vreven, T.; Kudin, K. N.; Burant, J. C.; Millam, J. M.; Iyengar, S. S.; Tomasi, J.; Barone, V.; Mennucci, B.; Cossi, M.; Scalmani, G.; Rega, N.; Petersson, G. A.; Nakatsuji, H.; Hada, M.; Ehara, M.; Toyota, K.; Fukuda, R.; Hasegawa, J.; Ishida, M.; Nakajima, T.; Honda, Y.; Kitao, O.; Nakai, H.; Klene, M.; Li, X.; Knox, J. E.; Hratchian, H. P.; Cross, J. B.; Bakken, V.; Adamo, C.; Jaramillo, J.; Gomperts, R.; Stratmann, R. E.; Yazyev, O.; Austin, A. J.; Cammi, R.; Pomelli, C.; Ochterski, J. W.; Ayala, P. Y.; Morokuma, K.; Voth, G. A.; Salvador, P.; Dannenberg, J. J.; Zakrzewski, V. G.; Dapprich, S.; Daniels, A. D.; Strain, M. C.; Farkas, O.; Malick, D. K.; Rabuck, A. D.; Raghavachari, K.; Foresman, J. B.; Ortiz, J. V.; Cui, Q.; Baboul, A. G.; Clifford, S.; Cioslowski, J.; Stefanov, B. B.; Liu, G.; Liashenko, A.; Piskorz, P.; Komaromi, I.; Martin, R. L.; Fox, D. J.; Keith, T.; Al-Laham, M. A.; Peng, C. Y.; Nanayakkara, A.; Challacombe, M.; Gill, P. M. W.; Johnson, B.; Chen, W.; Wong, M. W.; Gonzalez, C.; Pople, J. A. *Gaussian 03*, revision C.02; Gaussian, Inc.: Wallingford, CT, 2004.

(13) (a) Bally, T.; Borden, W. T. *Rev. Comput. Chem.* **1999**, *13*, 1. (b) Naumov, S.; Janovský, I.; Knolle, W.; Mehnert, R. *Nucl. Instrum. Methods Phys. Res. B* **2003**, *208*, 385−38.

(14) Williams, F.; Qin, X.-Z. *Radiat. Phys. Chem.* **1988**, *32*, 299.

(15) (a) Fessenden, R. W.; Schuler, R. H. *J. Chem. Phys.* **1963**, *39*, 2147. (b) Cochran, E. L.; Adrian, F. J.; Bowers, V. A. *J. Chem. Phys.* **1964**, *40*, 213. (c) Kasai, P. H.; Whipple, E. B. *J. Am. Chem. Soc.* **1967**, *89*, 1033.

(16) (a) Sprague, E. D.; Williams, F. *J. Am. Chem. Soc.* **1971**, *93*, 787. (b) Wang, J.-T.; Williams, F. *J. Am. Chem. Soc.* **1972**, *94*, 2930. (c) Campion, A.; Williams, F. *J. Am. Chem. Soc.* **1972**, *94*, 7633. (d) Le Roy, R. J.; Sprague, E. D.; Williams, F. *J. Phys. Chem.* **1972**, *76*, 546. (e) Hudson, R. L.; Shiotani, M.; Williams, F. *Chem. Phys. Lett.* **1977,** *48*, 193. (f) Le Roy, R. J.; Murai, H.; Williams, F. *J. Am. Chem. Soc.* **1980**, *102*, 2325. (g) Brunton, G.; Griller, D.; Barclay, L. R. C.; Ingold, K. U. *J. Am. Chem. Soc.* **1976**, *98*, 6803. (h) Brunton, G.; Gray, J. A.; Griller, D.; Barclay, L. R. C.; Ingold, K. U. *J. Am. Chem. Soc.* **1978**, *100*, 4197. (i) Toriyama, K; Nunome K.; Iwasaki, M. *J. Am. Chem. Soc.* **1977**, *99*, 5823.

(17) (a) Bell, R. P. *The Tunnel Effect in Chemistry*; Chapman and Hall: London, 1980; pp 106−114. (b) Grigoriev, E. I.; Trakhtenberg, L. I. *Radiation−Chemical Processes in Solid Phase: Theory and Application*; CRC Press: Boca Raton, FL, 1996; Chapter 4, pp 57−92.

(18) The temperature dependent spectra reported recently (Liu, W.; Yamanaka, S.; Shiotani, M.; Michalik, J.; Lund, A. *Phys. Chem. Chem. Phys.* **2000**, *2*, 2515) for some amine radical cations ($R_3N^{\bullet+}$) were attributed to the averaging of non-equivalent CH_3 or β-CH_2 1H splittings. In contrast to our results, where significant averaging of the N anisotropy is clearly evident from the outermost wings, no averaging of the N anisotropy was observed even at room temperature, pointing to different modes of interaction in the zeolite matrices.

(19) Shiotani, M.; Sjöqvist, L.; Lund, A.; Lunell, S.; Eriksson, L.; Huang, M.-B. *J. Phys. Chem.* **1990**, *94*, 8081.

(20) Naumov, S.; Janovský, I.; Knolle, W.; Mehnert, R. *Phys. Chem. Chem. Phys.* **2004**, *6*, 3933.

(21) (a) Cummings, C. B.; Bleakney, W. *Phys. Rev.* **1940**, *58*, 787. (b) Williams, T. F. *Nature* **1962**, *194*, 348.